Supporting Online Material for

A Rubberlike Stretchable Active Matrix Using Elastic Conductors

Tsuyoshi Sekitani, Yoshiaki Noguchi, Kenji Hata, Takanori Fukushima, Takuzo Aida,
Takao Someya*

*To whom correspondence should be addressed. E-mail: someya@ap.t.u-tokyo.ac.jp

This PDF file includes:

Materials and Methods
Figs. S1 to S14
References

Supporting Online Material

A Rubber-like Stretchable Active Matrix Using Elastic Conductors

Tsuyoshi Sekitani[1], Yoshiaki Noguchi[1], Kenji Hata[2], Takanori Fukushima[3,4,§], Takuzo Aida[3,4] ,

and Takao Someya[1,5] [*]

[1] *Quantum-Phase Electronics Center, School of Engineering, The University of Tokyo, 7-3-1*

Hongo, Bunkyo-ku, Tokyo 113-8656, Japan

[2] *Research Center for Advanced Carbon Materials, National Institute of Advanced Industrial*

Science and Technology, Tsukuba 305-8565 Japan

[3] *Department of Chemistry and Biotechnology, School of Engineering, The University of Tokyo*

7-3-1 Hongo, Bunkyo-ku, Tokyo 113-8656, Japan

[4] *Nanospace Project, Exploratory Research for Advanced Technology–Solution Oriented*

Research for Science and Technology, Japan Science and Technology Agency, National Museum

of Emerging Science and Innovation, 2-41 Aomi, Koto-ku, Tokyo 135-0064, Japan.

[5] *Collaborative Institute for Nano Quantum Information Electronics (INQIE), The University of*

Tokyo, 4-6-1, Komaba, Meguro-ku, Tokyo 153-8505 Japan

[*]Correspondence should be sent to Takao Someya (someya@ap.t.u-tokyo.ac.jp).

[§]Present address: Advanced Science Institute, RIKEN, 2-1 Hirosawa, Wako, Saitama 351-0198,

Japan

MATERIALS AND METHODS

1. Deformation of perforated films (Fig. S1)

Perforated films with a net-shaped structure were produced using a mechanical punching system (MP-8200Z, UHT Corporation). Stretch tests were performed using a high-precision mechanical system (AG-X, Shimadzu Corporation). The shape of the holes in the perforated films changed during stretching. The enhancement of stretchability on perforated films is realized because the interconnecting struts buckle and twist out-of-plane upon tension. Fig. S1 shows the top and side views of perforated films under different tensile strains; the photographs were taken with a digital camera.

The maximum stretchability of the net-shaped structure depends on the roundness of the corners having the holes as well as on the hole geometries and the modulus of resilience. For example, polyethylene naphthalate (PEN) films are semi-rigid and cannot be stretched; however, perforated PEN films with a thickness of 150 μm and similar hole geometries can be stretched up to 30~35%. Due to similar mechanisms, the stretchability of the net-shaped elastomer can be improved significantly.

The degree of stretchability and the apparent modulus depend on the direction of the strain relative to the struts that form the boundaries of the holes and the overall geometry. In the net-shaped elastic conductors with the PDMS coating, the struts are 0.6~1.0 mm in width and 150~250 μm in thickness. The periodicity of the boundaries of the holes is 5.04 mm, which is determined by the periodicity of the organic transistors. By reducing the width of the struts, we

could improve the mechanical performance of the conductors, while the conductance decreased. Therefore, the overall geometry of the system has to be designed carefully so that both the mechanical and the electric performances meet the requirements for the specific applications.

2. Electrical characteristics under tensile strains.

For both SWNT films without a PDMS coating and elastic conductors (SWNT films coated with PDMS), we measured the conductance by using the typical four-probe method with a high-precision multimeter. The effective length and width of the SWNT films acting as the conducting parts were measured by using a digital vernier caliper, while the thickness was measured by using both a digital microscope and a digital vernier caliper. After carrying out these measurements for each tensile strain value considered in the study, we converted each conductance to conductivity.

3. Optimization of fabrication of SWNT films

3-1. Compatibility test (Fig. S2)

(A) Images of gels mixed with fluorinated copolymer as base polymer matrix, G801, and different kinds of ionic liquids for examining the compatibility. 1-Butyl-3-methylimidazolium bis(trifluoromethanesulfonyl)imide (BMITFSI), 1-butyl-3-methylimidazolium hexafluorophosphate (BMIPF$_6$), and 1-butyl-3-methylimidazolium tetrafluoroborate (BMIBF$_4$) were used as ionic liquids. As shown in Fig. S2A, BMITFSI was compatible with G801. When SWNT, BMITFSI, and G801 were mixed, the SWNT films were smooth and exhibited high conductivity. On the other hand, when other ionic liquids were used, the SWNT films were deformed or crumpled (Fig. S2B). When imidazolium-ion-based room temperature ionic liquid

BMITFSI was employed, entangled SWNT bundles resolved into much finer bundles or individual nanotubes, thereby yielding bucky gel successfully. Images of the surfaces of SWNT films are shown in Fig. S2C; these images were obtained by scanning electron microscopy (SEM). Because of the uniform dispersion of SWNTs in a polymer matrix, the conductivity of SWNT films with ionic liquids was considerably higher than that of SWNT films without ionic liquids, as shown in Fig. S3.

3-2. Change in conductivity of SWNT films with change in content of base polymer G801 (Fig. S3)

The conductivity of SWNT films with ionic liquids was considerably higher than that of SWNT films without ionic liquids. For elastic conductors manufactured by mixing SWNTs and a fluorinated copolymer G801, the conductivity increased to as high a value as 30 S/cm. However, such SWNT copolymers without ionic liquids had fragile and porous membranes, and they did not exhibit elasticity and flexibility. When the filling factor of SWNTs was increased to improve the conductivity, the stretchability decreased significantly (see Fig. S6). The SEM images clearly indicate that entangled SWNT bundles were resolved into much finer bundles or individual nanotubes using ionic liquids. Such a homogeneous dispersion of SWNTs leads to higher conductivity.

3-3. Content dependence of conductivity and membrane

3-3-1 Content of ionic liquid BMITFSI (Fig. S4)

Each sample shown in Fig. 2E was examined by (B) optical microscopy and (C) scanning electron microscopy (SEM). Figure S4A is retraced from Fig. 2E together with the sample

number. The quality of the membrane significantly depended on the content of BMITFSI. When the content ratio of BMITFSI was more than 40 wt%, the SWNT film became a discontinuous membrane. When the ratio was less than 10 wt%, the films were thick, porous, and fragile membranes and exhibited low conductivity. The SEM images show that when the content of BMITFSI was 10 wt%, the SWNTs were still entangled and they formed bundles. However, entangled SWNT bundles could be resolved into finer bundles as the content of BMITFSI increased.

3-3-2 Content of SWNT (Fig. S5)

Similar experiments were performed by changing the content of SWNT. Figure S5A is retraced from Fig. 2F together with the sample number. Optical microscopy and SEM images are shown in Figs. S5B and C. The SEM images show that the films are porous membranes when the content of SWNTs increases.

3-4. Change in content dependence with change in mixing ratio of SWNT and BMITFSI (Fig. S6)

The SWNT films were electrically and mechanically characterized by changing the mixing ratio of SWNT and BMITFSI. The thickness, conductivity, breaking stress, and critical tensile strain of SWNT films are plotted in Figs. S6A–D, respectively, as a function of the bucky gel content in milligrams. The mixing ratios of the SWNT and BMITFSI were set to 2:1, 1:1, or 1:2. The thickness monotonically increased with the content of bucky gels comprising SWNTs and BMITFSI (Fig. S6A). However, the conductivity did not always increase with the bucky gel content. From Fig. S6B, we found that a higher conductivity could be obtained when the amount

of SWNT was equivalent to that of BMITFSI. When the mixing ratio of SWNT and BMITFSI was 1:1, the conductivity of the SWNT films increased monotonously with the bucky gel content and exceeded 50 S/cm when the content of bucky gels was approximately 30 wt%. The conductivity strongly depends on the content of SWNT and BMITFSI in the bucky gels. When the contents of SWNT and BMITFSI were approximately 15~20 wt%, the highest conductivity was obtained. However, further increase in the bucky gel content caused a reduction in conductivity because the films became fragile and porous membranes (Fig. S6C). The critical tensile strain after changing the mixing ratio of SWNT and BMITFSI is shown in Fig. S6D. The stretching test was performed using a high-precision mechanical system (AG-X, Shimadzu Corporation), while electrical characteristics were measured using typical four probe method.

3-5. Tensile strain vs. mechanical properties of SWNT films (Fig. S7)

The breaking stresses of SWNT films are shown as a function of the tensile strain at different SWNT contents. SWNT contents were changed as follows: 4.5%, 8.3%, 11.5%, 17%, 22.2%, 25%, and 37.5%. The contents of ionic liquid, BMITFSI, were the same as those of SWNT; in other words, the mixing ratio of SWNT and BMITFSI was 1:1, while the amount of G801 was 100 mg. When the content was approximately 10~20 wt%, the durability under tensile strains was found to be more than 6 N/mm^2.

3-6. Aspect ratio of SWNTs (Fig. S8)

Films with the super-growth SWNTs (>1 mm in length and 3 nm in diameter) typically exhibited a conductivity in excess of 40 S/cm when the materials and content were optimized. The average conductivity of the films with commercially available HiPco SWNTs was lower than that of

films with the super-growth SWNTs by a factor of two or three. This result indicates that a high aspect ratio of carbon nanotubes is important to obtain higher conductivity.

3-7. Tensile strain vs. mechanical properties of SWNT paste (Fig. S9)

Breaking stresses of SWNT paste are shown as a function of tensile strain. The manufacturing process and the electrical characteristics are described in the text. The strength of adhesion was found to be 1.5 N/mm^2, which is sufficient for forming interconnections between elastic conductors and electrodes for organic transistors.

4. Stretchable active matrix

4-1. Manufacturing process of printed organic transistors

Organic transistors were manufactured using inkjet printing (Ricoh Printing Systems Co., Ltd.; IJP-1), screen printing (Micro-tec Co., Ltd.; MT-550), and vacuum evaporation methods. The base film (substrate) was a polyimide film with a thickness of 75 μm. Ag nanoparticles (Harima Chemical Co., Ltd.; NPS-J-HP) were patterned by inkjet printing and cured at 180 °C to form 300-nm-thick gate electrodes. Epoxy partitions were formed around the gate electrodes by using screen printing. Diluted polyimide precursors (Kyocera Chemical Co., Ltd.; KEMITITE CT4112) were ink-jetted and cured at 180 °C to form 1-μm-thick polyimide gate dielectric layers. Ag nanoparticles were patterned by inkjet printing and cured at 180 °C to form source and drain electrodes. A 50-nm-thick pentacene layer was deposited using vacuum evaporation with rotation mechanics through printed shadow masks (*S1*) to form a channel layer. The channel length and width were typically 150 μm and 6 mm, respectively. Finally, a 5-μm-thick layer of poly-chloro-para-xylylene, i.e., parylene (Daisankasei Co., Ltd.; diX-SR), was uniformly coated

to form a passivation layer. The fabrication process is similar to the method reported in the literature (*S2*). The stand-alone manufactured organic transistors exhibited a mobility of 0.3~1.0 cm^2/Vs and an on/off ratio of 10^7.

4-2. Mechanical punching process and integration of SWNT elastic conductor (Fig. S10)

The manufacturing process of the large-area stretchable active matrix using printing technologies and the mechanical punching process is shown in Fig. S10. (A) First, organic transistors were manufactured using inkjet printing, screen printing, and vacuum evaporation with rotation mechanics; this process is described in detail in the literature (*S2*). (B) Parts of the films except for the part with the organic transistors were punched out using a mechanical punching system (MP-8200Z, UHT Corporation). It should be noted that in this process, the transistors were still physically connected to the edges of the four corners. (C) The punched transistor sheet was stacked on 500-μm-thick silicone rubbers prepared beforehand. In this work, we used two types of silicone rubbers (PDMS): one is the popular dimethyl-siloxane-based rubber, named Sylgard 184 (Dow-Corning Toray Co., Ltd., Young's modulus: 6 MPa (6 N/mm^2)), which is transparent and whose maximum stretchability is 120%, and the other is also a dimethyl-siloxane-based rubber, named SH9555 (Dow-Corning Toray Co., Ltd., Young's modulus: 6 MPa (6 N/mm^2)), which is white in color and whose maximum stretchability is 440% as per the specification sheet. (D) The edges of each transistor placed on a PDMS sheet were mechanically punched out to isolate the transistors. (E) Via holes for interconnections among the gate, source, and drain electrodes of the transistors were formed by using the punching system, and the diameter of these via holes was 1 mm. Then, by employing a microdispenser, the via holes were filled with droplets of Ag paste. The paste was dried at room temperature in air to form the contact pads of

the gate, source, and drain electrodes. (F) SWNT elastic conductors in the form of word lines were fixed on the contact pads of each gate electrode to form interconnections among the gate electrodes of the transistors. (G) SWNT elastic conductors in the form of bit lines were fixed on the contact pads of each source electrode to form interconnections among the source electrodes of the transistors. Finally, the entire assembly was coated with PDMS and cured at 60 °C, which resulted in a PDMS encapsulation with a thickness of 500 μm. The top surfaces of the word lines and bit lines were coated with PDMS; therefore, these lines were electrically isolated.

4-3. Via interconnection between organic transistors and SWNT elastic conductor (Fig. S11)

(A) and (B) Typical transistor characteristics of the discrete transistors (before interconnection using SWNT elastic conductor). The channel width and length of the transistors were 2 mm and 150 μm, respectively. (C) Transfer characteristics of typical transistors before and after integrating SWNT elastic conductor, represented by red and green lines, respectively. The via holes of the transistors were filled with Ag paste and connected to the SWNT elastic conductor electrically and mechanically through SWNT paste. No damage or change was observed even after the integration. The typical characteristics of organic transistors with via holes filled with SWNT paste (blue line) are also shown for comparison. Images of the top view and cross section are shown. A large decrease in the channel currents was observed when the SWNT paste was used as the material for filling the via holes since there was no path for vaporizing the organic solvent, although the SWNT paste required the drying of an organic solvent. This result clearly demonstrates that residual organic solvents affect the electrical characteristics. In contrast, excellent electrical characteristics were acquired using SWNT-based materials when the organic

solvent was eliminated completely.

4-4. Electrical characteristics after integration (Fig. S12)

Stand-alone organic transistors (before wiring using SWNT elastic conductor) and their active matrices (after wiring) were characterized for evaluating the electrical functionalities of the manufactured SWNT elastic conductor on a large-scale matrix. As shown in Fig. S12, all the transistors were functional after interconnecting the organic transistors wired using the SWNT elastic conductor. (A) Transfer characteristics of 64 discrete transistors (before wiring, blue lines) and transistors formed as an active matrix using SWNT elastic conductor (after wiring, red lines). The channel width and length of the transistors were 6 mm and 150 μm, respectively. The changes in (B) saturation currents, (C) field-effect mobilities evaluated in the saturation regime, and (D) on/off ratios are shown. The dashed lines represent average values. Histograms before and after wiring are also shown. The mobilities decreased by 50%, which may be due to the effect of the coating of PDMS on the transistors and partially due to air degradation during several process steps. The on/off ratio also decreased from 10^7 to 10^6 after the interconnections were formed. Such a reduction in the on/off ratio was generally observed when transistors were wired to each other using word lines and bit lines since a small leakage current (typically less than 100 pA) was added for every row and column, although all the elastic conductors were coated with PDMS. The suppression of such leakage currents is necessary when there is an increase in the number of transistors. One of the possible processes for suppressing leakage is forming an insulating paste by screen printing.

4-5. Recovery performance after stretching (Fig. S13)

10

The sheet was stretched by increasing the tensile strain and the extension distortion was released. Figure S13 shows the transistor characteristics and channel currents (I_{DS}) after the release of uniaxial and biaxial stretching up to 100%. The I_{DS} values were normalized by I_{DS} measured before the experiments as the initial state. The change in transistor performance was negligibly small up to 80% tensile strain, indicating excellent robustness of the present device under stretching.

5. Resistances of organic transistors in on state and word and bit lines (Fig. S14)
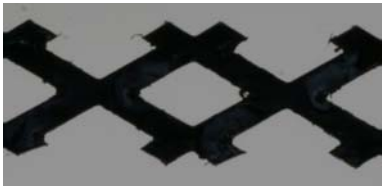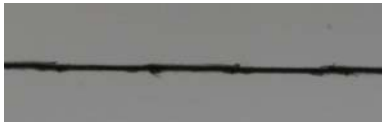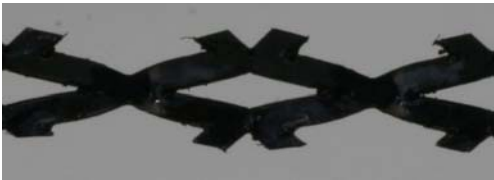
The resistances of the word and bit lines affect the electrical characteristics of transistors in an active matrix. When the resistance of transistors in the on state is comparable to that of the word and bit lines, the channel currents degrade. As shown in the table in Fig. S14, we manufactured five transistors with different channel widths and lengths. The resistances of the transistors in the on state (R_{ON}) were changed as follows: 3.3 MΩ, 200 KΩ, 40 KΩ, 9.2 KΩ, and 4.3 KΩ. The source, drain, and gate electrodes of these transistors were connected to the resistances, which were assumed as parasitic resistances (R_P), on the wiring interconnecting the transistors in the active matrix, for example, the resistances of the word and bit lines. Figure S14A shows the circuit diagram for the experiment. On increasing R_P, the channel currents (I_{DS}) of these transistors degraded. The decrease in I_{DS} started when R_P was almost comparable to R_{ON}. Therefore, if transistors have a high mobility or very low R_{ON} or if the size of the transistor active matrix increases, a very low resistance (very high conductivity) of the word and bit lines is unavoidable.

A commercially available carbon-particle-based conducting rubber has a conductivity of 0.1

S/cm. If we assume the formation of a stretchable active matrix with a size of 1×1 m^2 using carbon-particle-based conducting rubber (conductivity: 0.1 S/cm), the word and bit lines are estimated to offer a resistance of 100 KΩ. In this case, the on resistance of the transistors, R_{ON}, is limited to considerably less than 100 KΩ. Furthermore, such a high resistance of the word and bit lines may result in a low-frequency response of the circuits. The degradations of electrical characteristics originated from high resistive conductors become significant when the resistance of the word and bit lines is larger than R_{ON}. An elastic conductor with high conductivity and high stretchability will be formed under such conditions.

REFERENCES

S1. Y. Noguchi, T. Sekitani, T. Someya, Appl. Phys. Lett. **91**, 133502 (2007).

S2. Y. Noguchi, T. Sekitani, T. Someya, Appl. Phys. Lett. **89**, 253507 (2006)

Strain	Top view	Side view
0%		
15%		
30%		

5.08 mm

Fig. S1. Deformation of perforated films under stretching.

(A)

Compatibility of ionic liquids with fluorinated copolymer, G801

BMIPF$_6$ BMIBF$_4$ BMITFSI
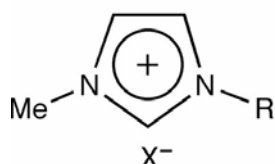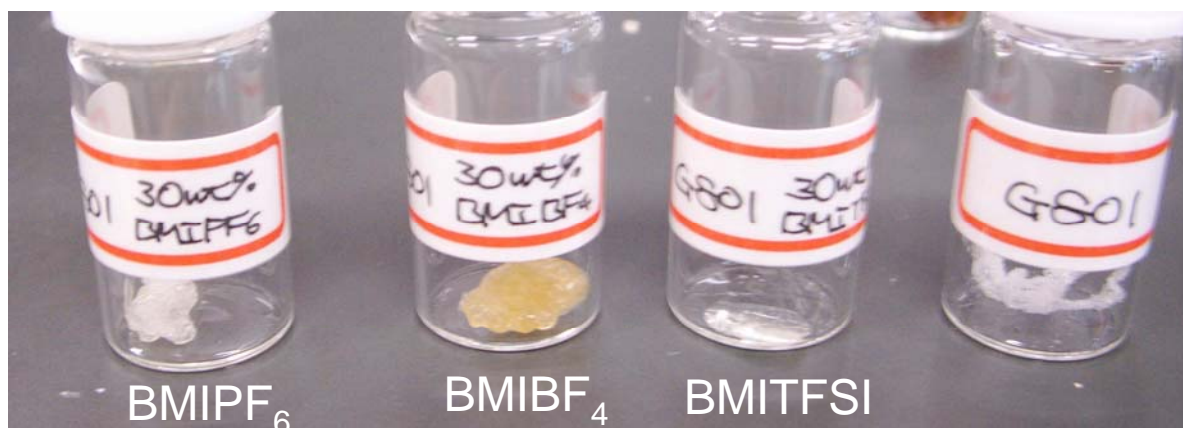
BMIBF$_4$: R = n-C$_4$H$_9$, X = BF$_4$

BMIPF$_6$: R = n-C$_4$H$_9$, X = PF$_6$

BMITFSI : R = n-C$_4$H$_9$, X = (CF$_3$SO$_2$)$_2$N

(B)

BMITFSI + G801   BMIBF$_4$ + G801   BMITFSI + KYNAR

20 mm

(C)
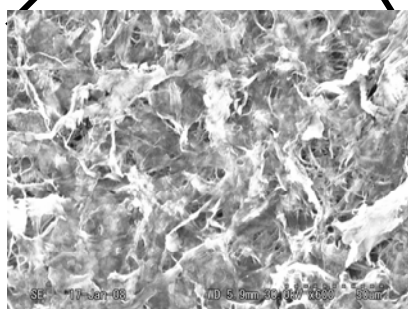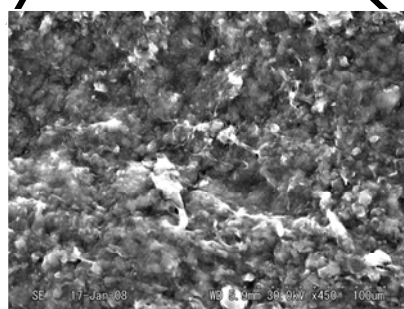
50 μm   50 μm

Fig. S2. (A) A picture of compatibility test. (B) Pictures of SWNT films with different material combination. (C) SEM images.
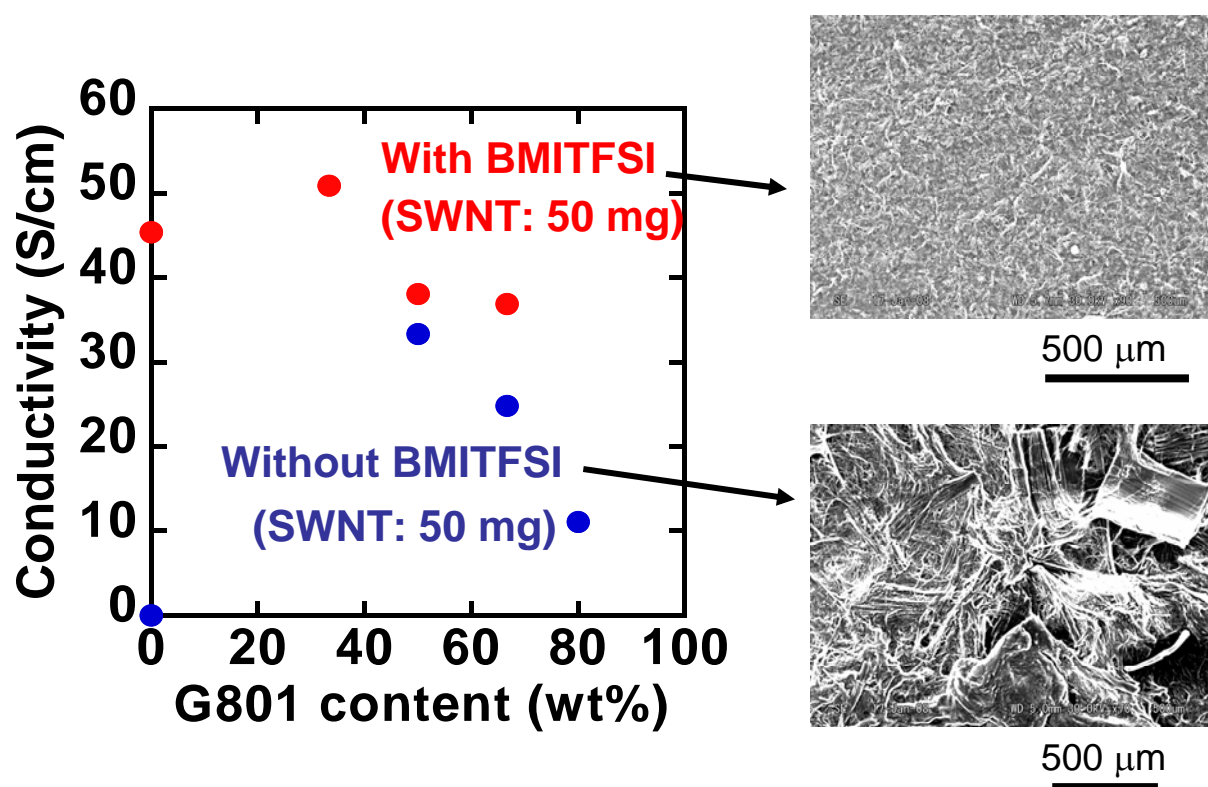
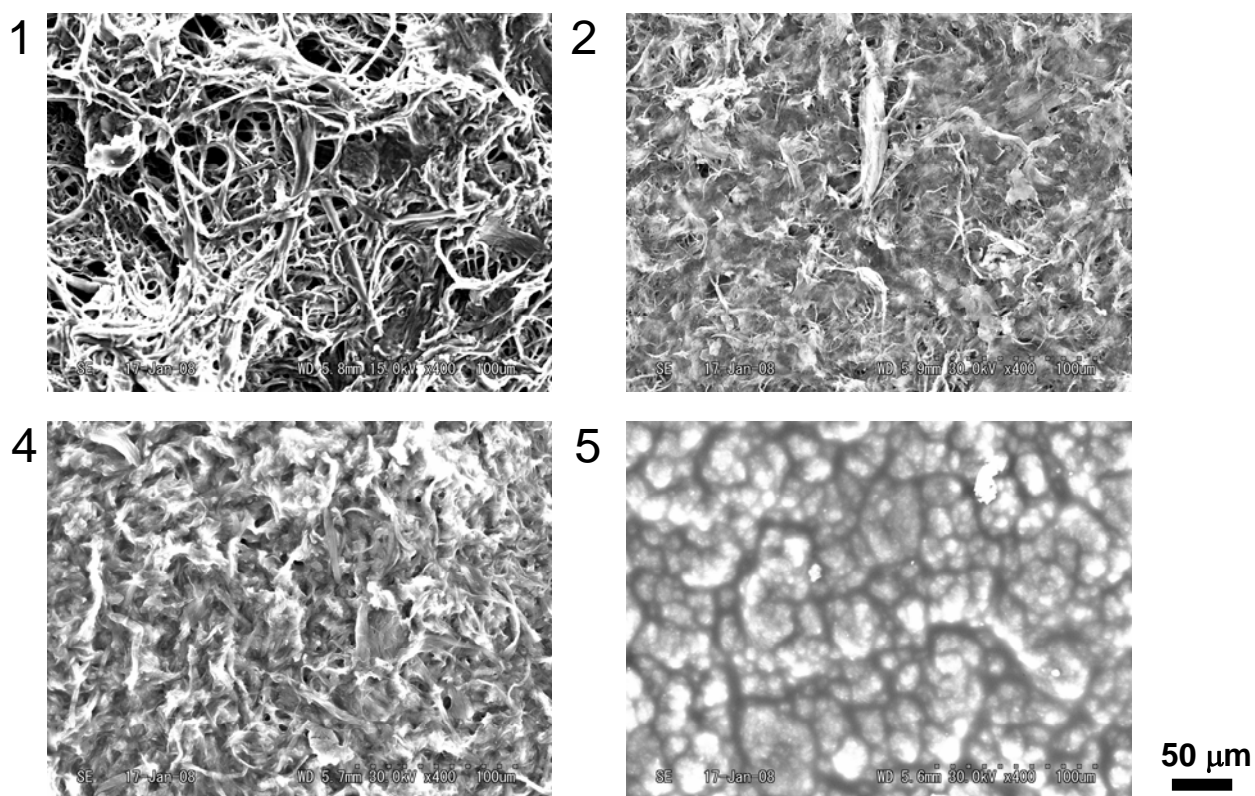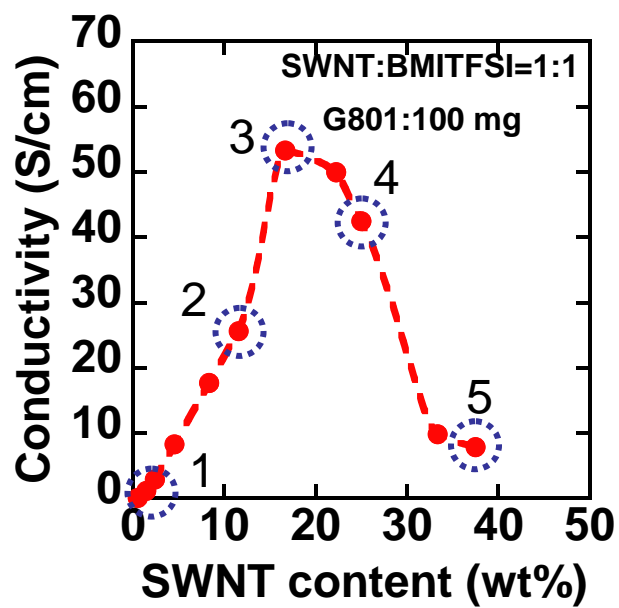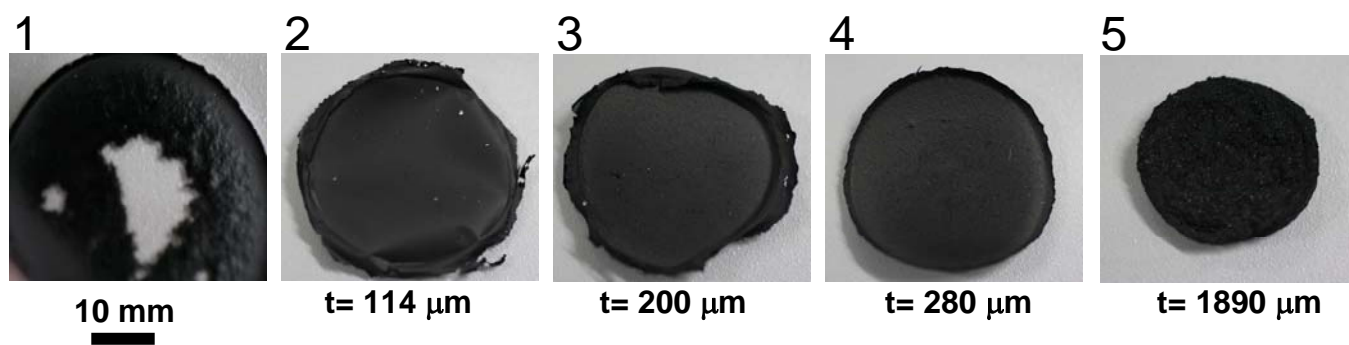Fig. S3. Change in conductivity of SWNT films with change in content of base polymer G801

(A)

SWNT: 50 mg
G801 : 100 mg

(B)

1 2 3 4 5

t= 312 μm   t= 260 μm   t= 240 μm   t= 140 μm

10 mm

(C)

1 2

4 5

50 μm
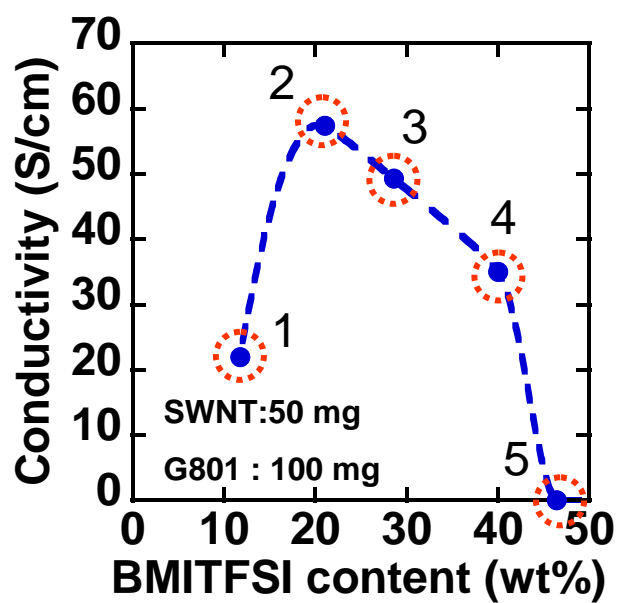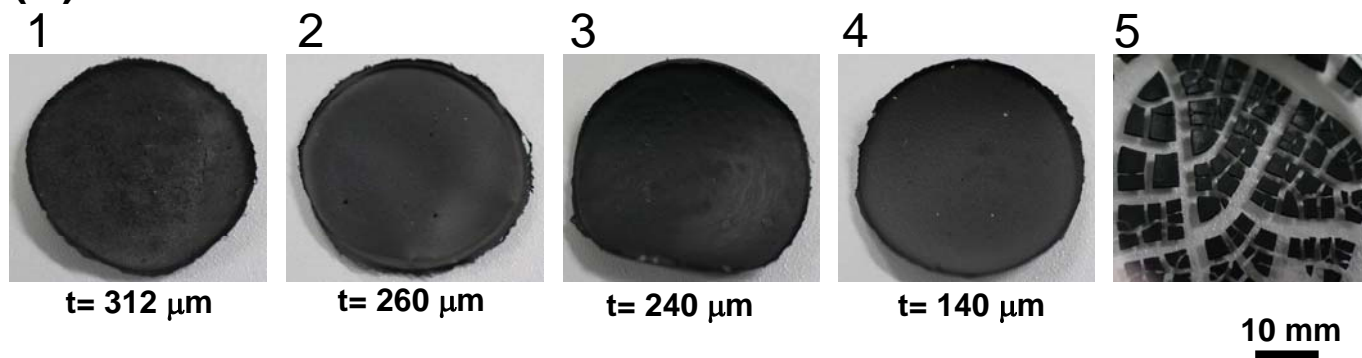
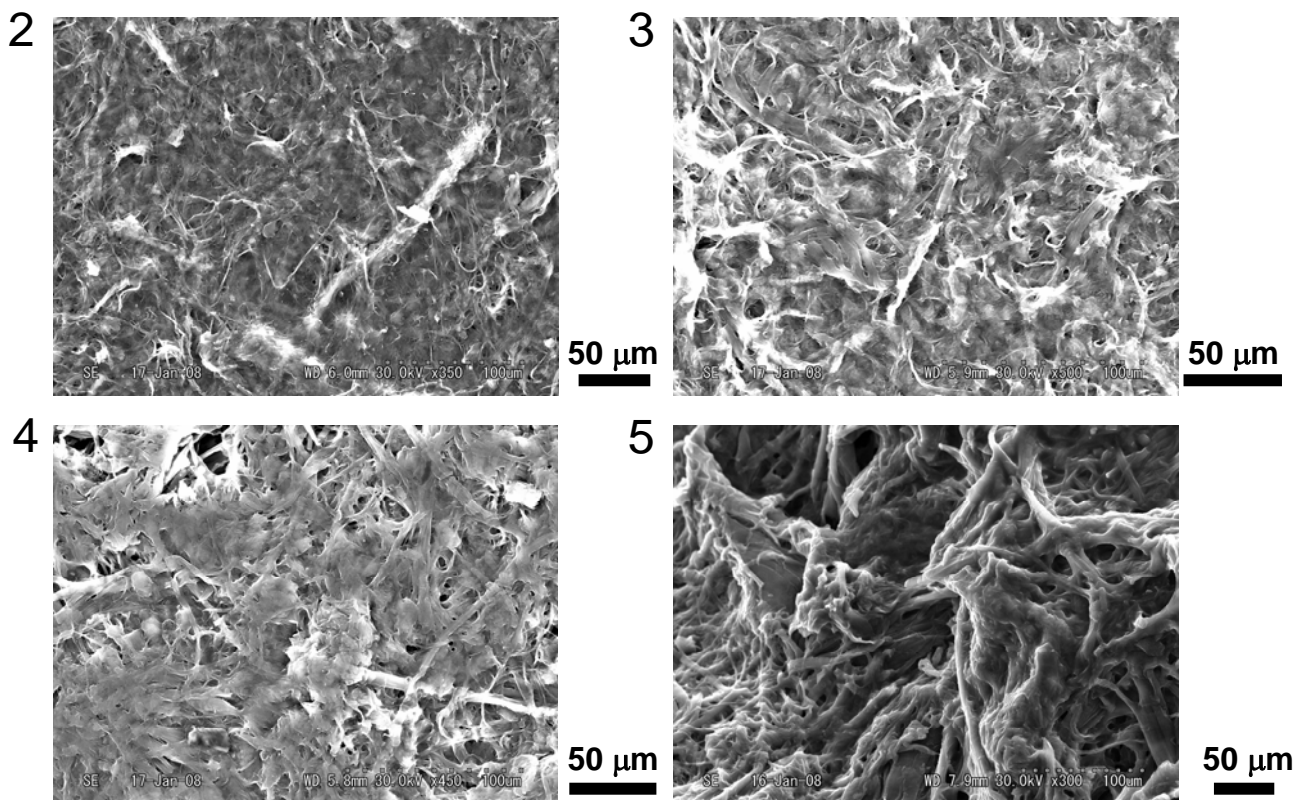Fig. S4. Content of ionic liquid BMITFSI.

(A)

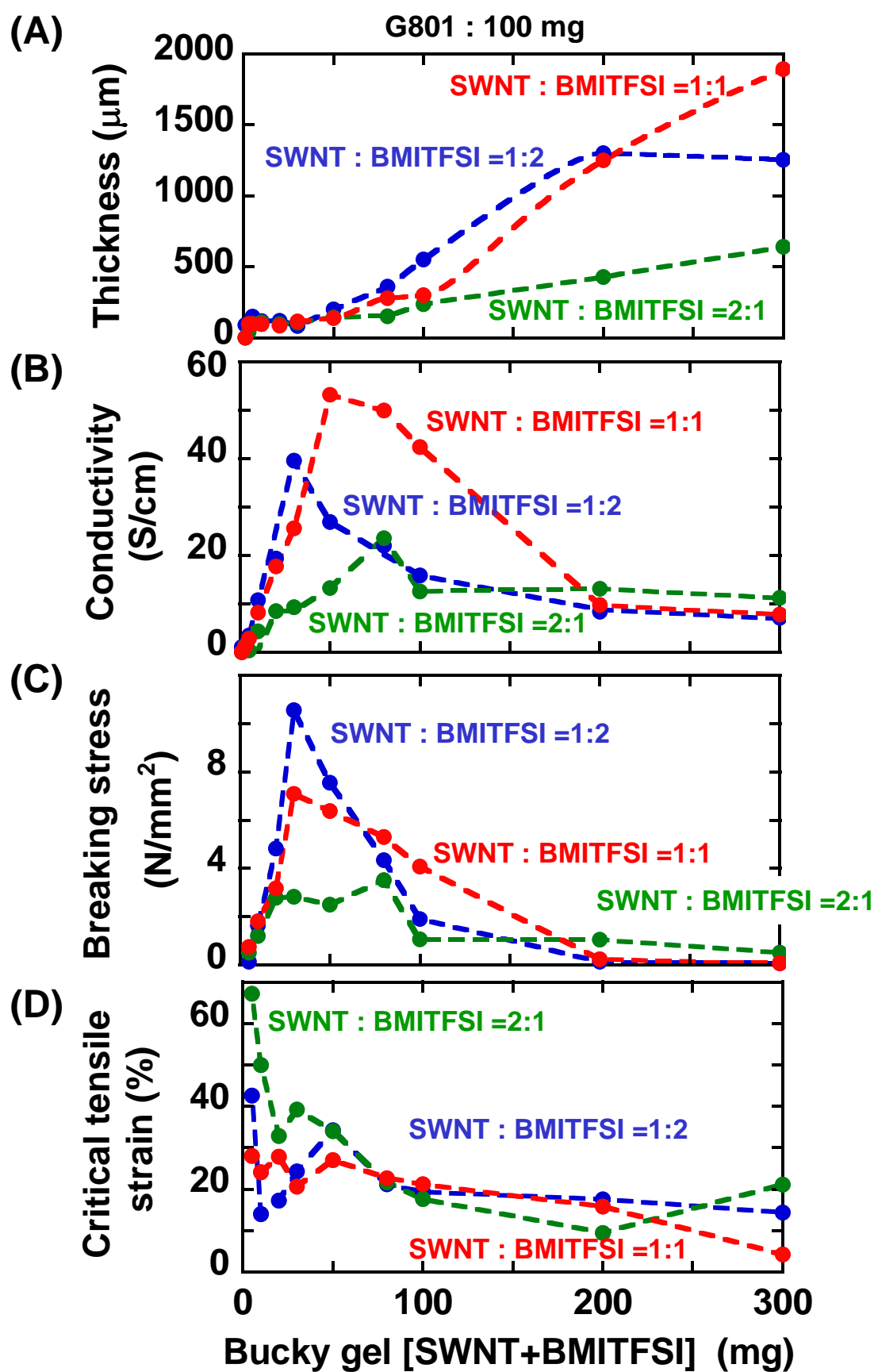

(B)

(C)

Fig. S5. Content of SWNT.

Fig. S6. Change in content dependence with change in mixing ratio of SWNT and BMITFSI.
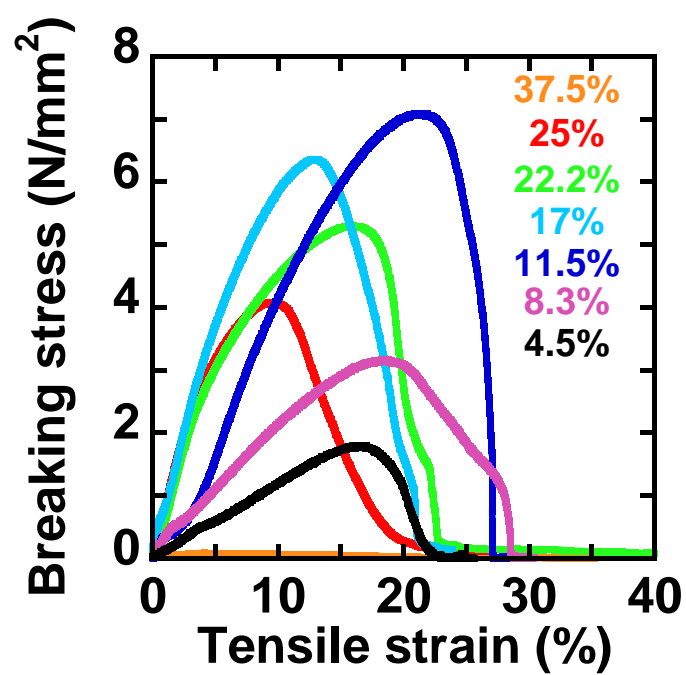
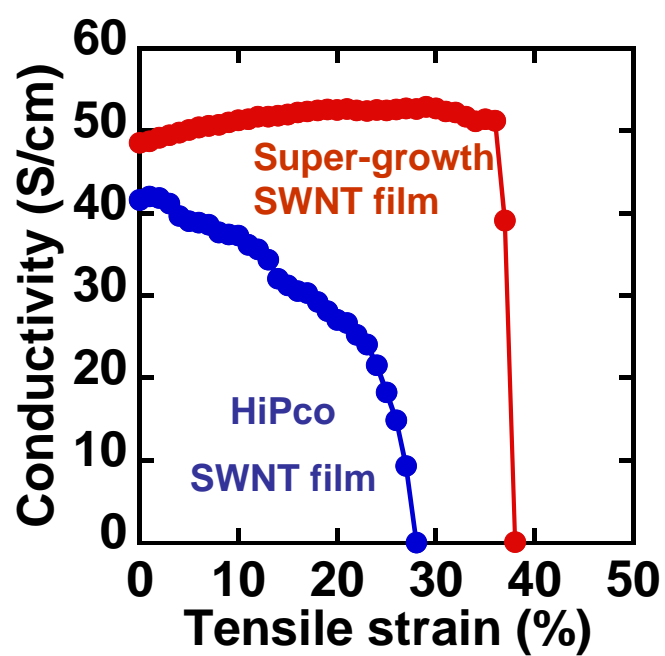Fig. S7. Tensile strain vs. mechanical properties of SWNT films.

Fig. S8. Conductivity of SWNT films as a function of tensile strain. SWNTs with different aspect ratio were used.
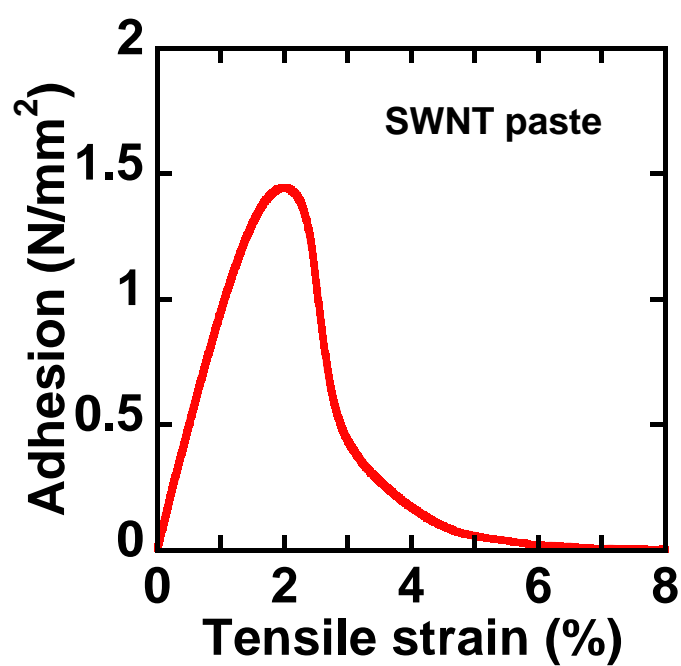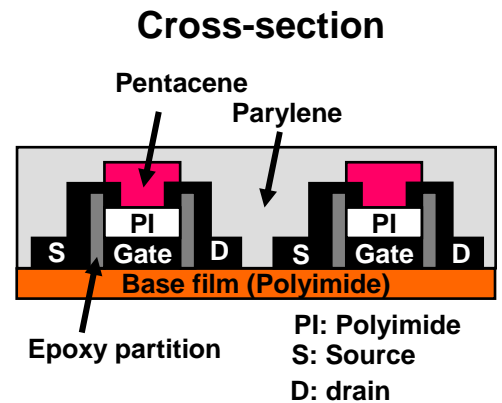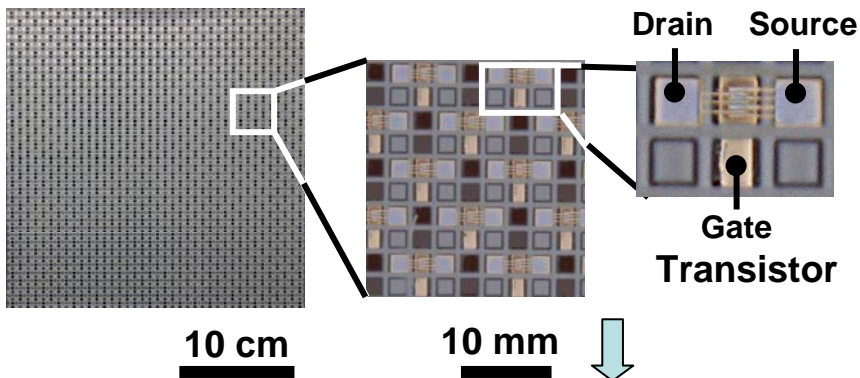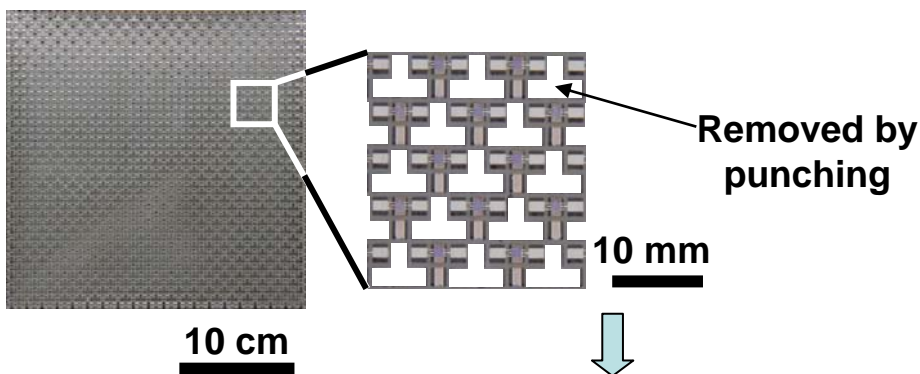
Fig. S9. Tensile strain vs. mechanical properties of SWNT paste.

Process steps

(A) Manufacturing of printed organic transistors

Drain **Source**

Gate
Transistor

10 cm

10 mm

Cross-section

Pentacene
Parylene

S   Gate   D   S   PI   Gate   D

PI

Base film (Polyimide)

Epoxy partition

PI: Polyimide
S: Source
D: drain

(B) Mechanical punching outside of the transistors

**Removed by
punching**

10 mm

10 cm

(C) Fix the punched transistors on PDMS sheet

PDMS

10 mm

Cross-section

S   PI   Gate   D   S   PI   Gate   D

Base film (Polyimide)
Base rubber (PDMS)
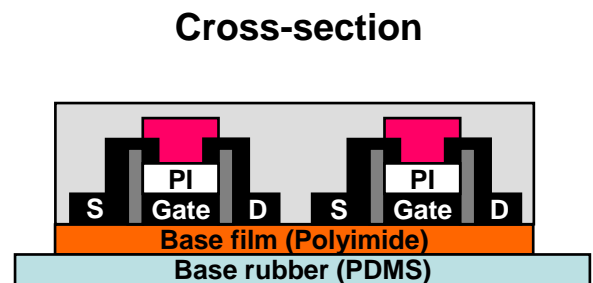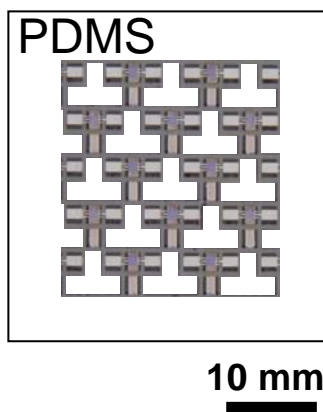
(D) Cut the connecting points to isolate the transistors

PDMS

**Removed by
punching**

10 mm

Cross-section

S   PI   Gate   D   S   PI   Gate   D

Base rubber (PDMS)
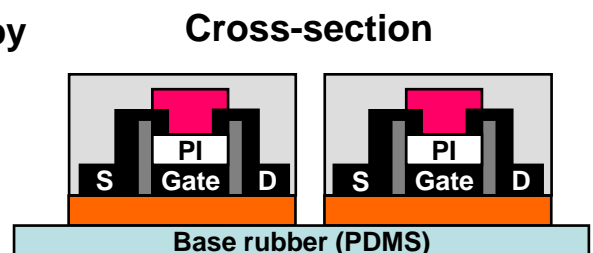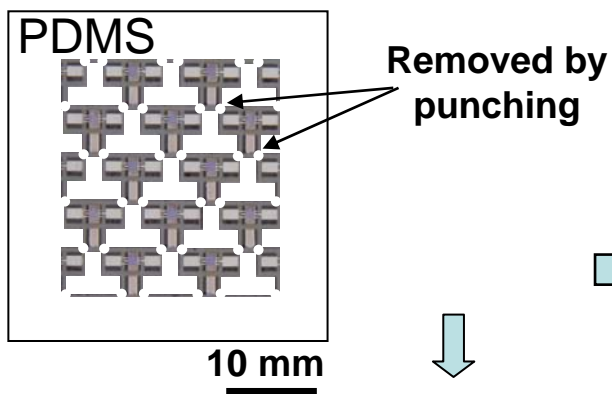
(E) Make via holes using punching and filled with Ag paste

PDMS

Ag paste

Cross-section

2 mm

10 mm

| Ag | | Ag | Ag | | Ag |
PI
S Gate D   S Gate D
Base rubber (PDMS)
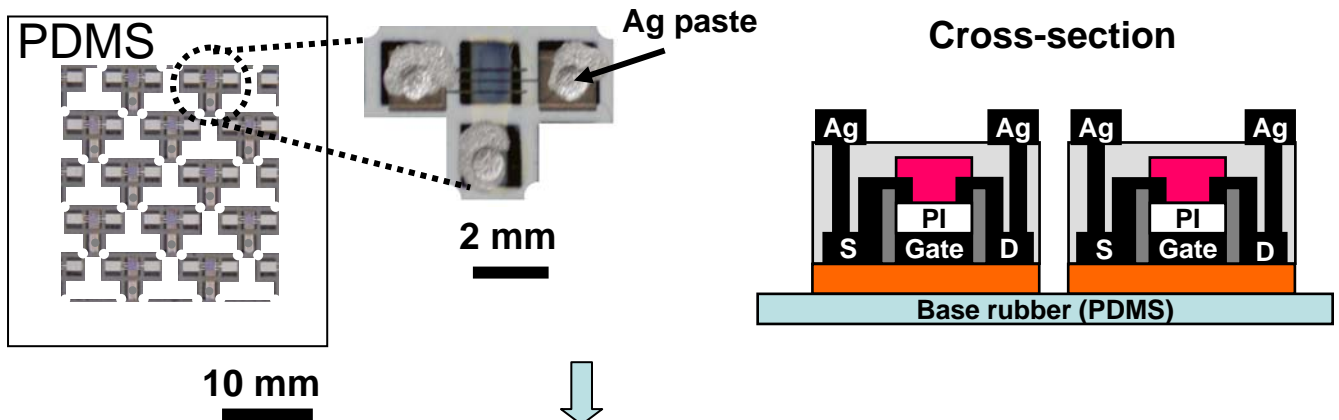
(F) Elastic conductors are fixed using SWNT pastes for the interconnections between word-lines and gate electrodes

PDMS

Word-line comprising elastic conductors

Cross-section

Ag | Ag   Ag | Ag
PI
S G●e D   S G●e D
Base rubber (PDMS)

Word-line

10 mm
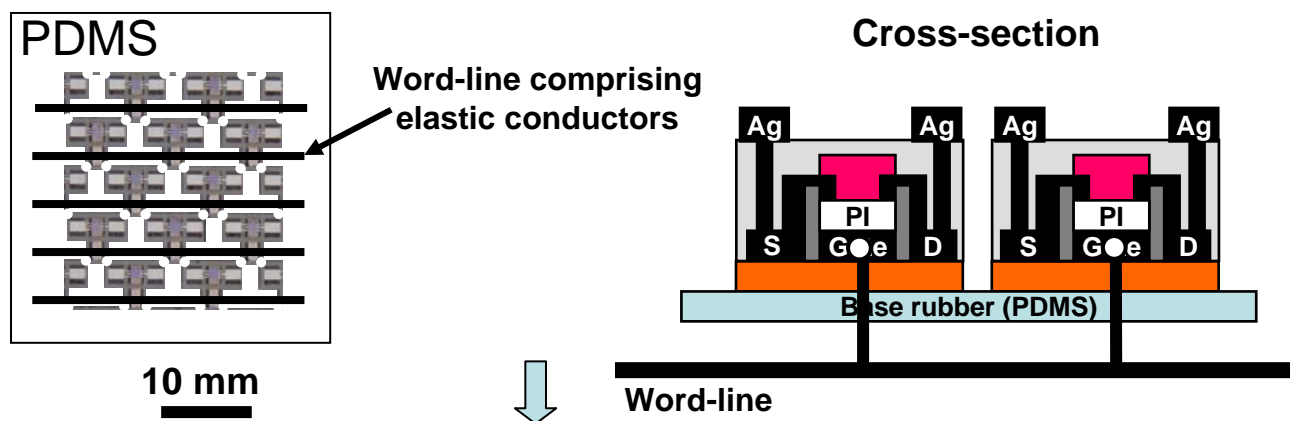
(G) Elastic conductors are fixed using SWNT pastes for the interconnections between bit-lines and source electrodes, and finally the whole of the device is coated with 500-μm-thick PDMS.

Cross-section

PDMS

Bit-line comprising elastic conductors

10 mm

Bit-line   Bit-line

Ag | Ag   Ag | Ag
PI   PI
S G●e D   S G●e D
Base rubber (PDMS)

Word-line
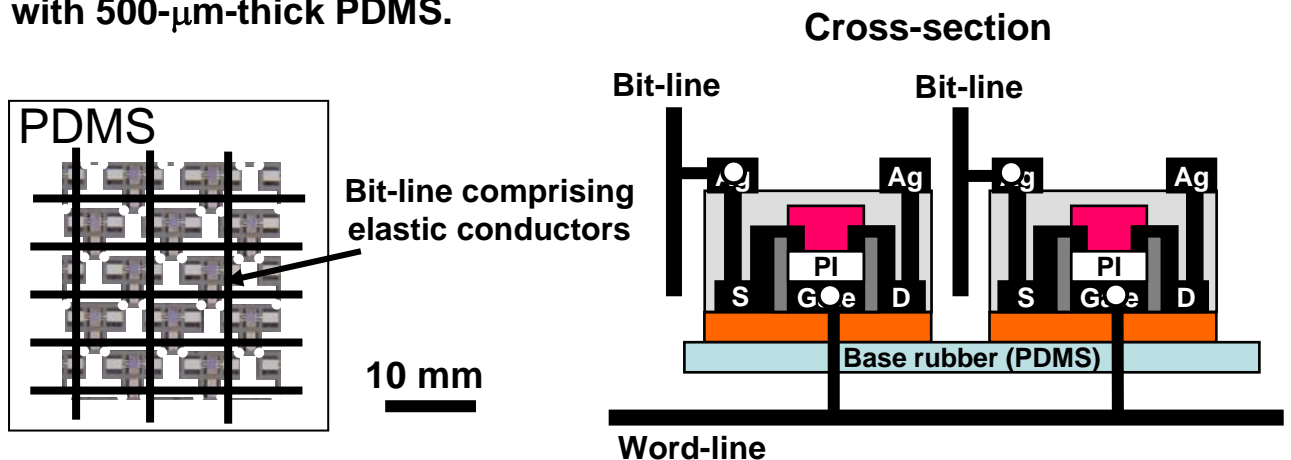
Note: The top surface of word- and bit-lines are coated with insulating PDMS, therefore these lines are isolated electrically.

Fig. S10. Manufacturing process of a stretchable active matrix.

(A)

V_{GS} = 0 to − 60 V
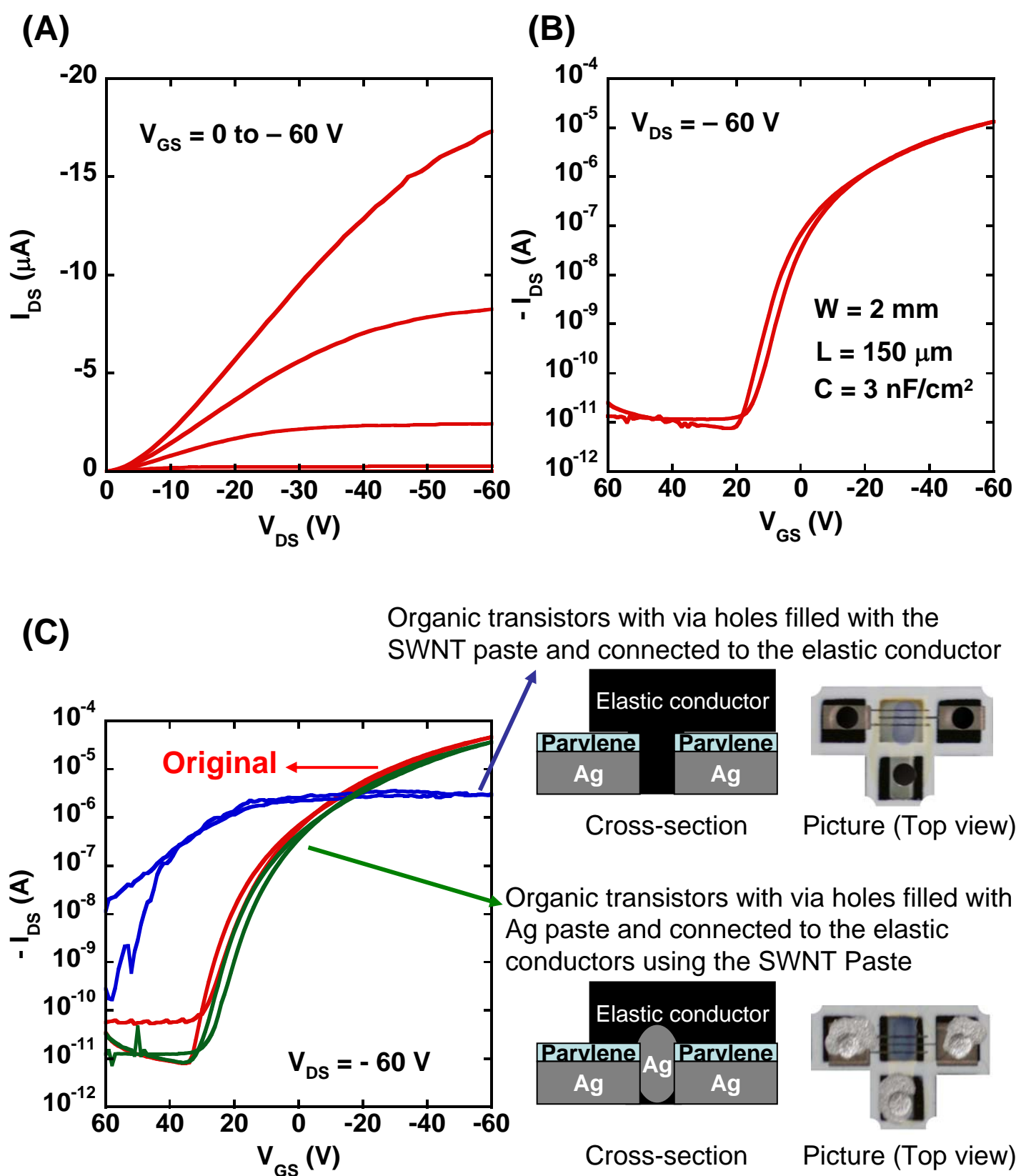
I_{DS} (μA) vs V_{DS} (V)

(B)

V_{DS} = − 60 V

W = 2 mm
L = 150 μm
C = 3 nF/cm²

− I_{DS} (A) vs V_{GS} (V)

(C)

Original

V_{DS} = − 60 V

− I_{DS} (A) vs V_{GS} (V)

Organic transistors with via holes filled with the SWNT paste and connected to the elastic conductor

Elastic conductor

Parvlene   Parvlene
Ag   Ag

Cross-section   Picture (Top view)

Organic transistors with via holes filled with Ag paste and connected to the elastic conductors using the SWNT Paste

Elastic conductor

Parvlene Ag Parvlene
Ag   Ag

Cross-section   Picture (Top view)

Fig. S11. Transistor characteristics of printed organic transistors

(A)

After wiring

Before wiring

$V_{DS} = -60$ V

W = 6 mm

L = 150 μm

C = 3 nF/cm^2

- I$_{DS}$ (A)

V$_{GS}$ (V)

(B)

On current (μA)

Before

After

Device No.

Number

Before

After

On current (μA)

(C)

Mobility (cm^2/Vs)

Before

After

Device No.

Number

Before

After

Mobility (cm^2/Vs)

(D)

ON/off ratio

Before

After

Device No.
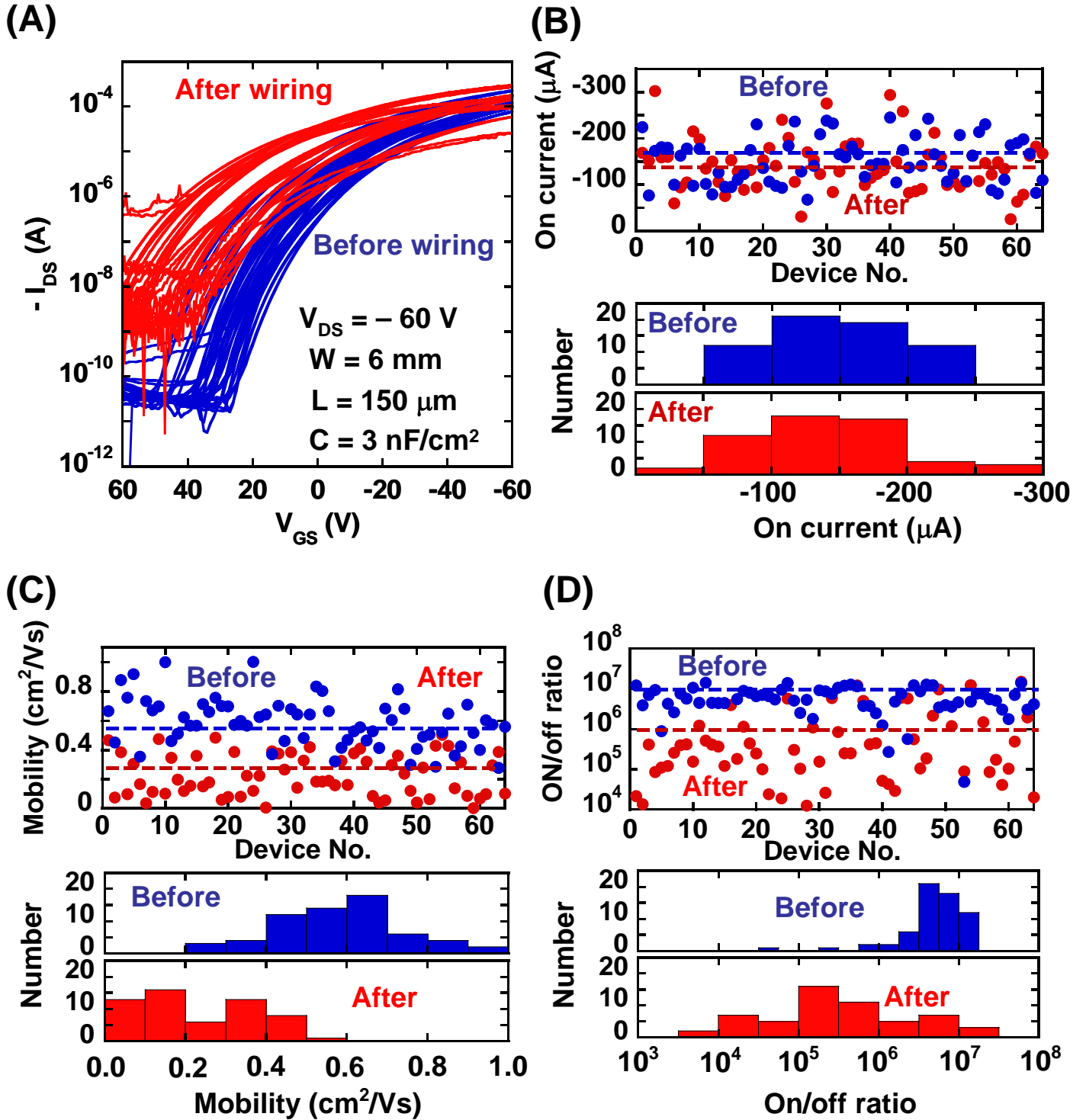
Number

Before

After

On/off ratio

Fig. S12. Comparison of electrical characteristics before and after wiring using elastic conductors.
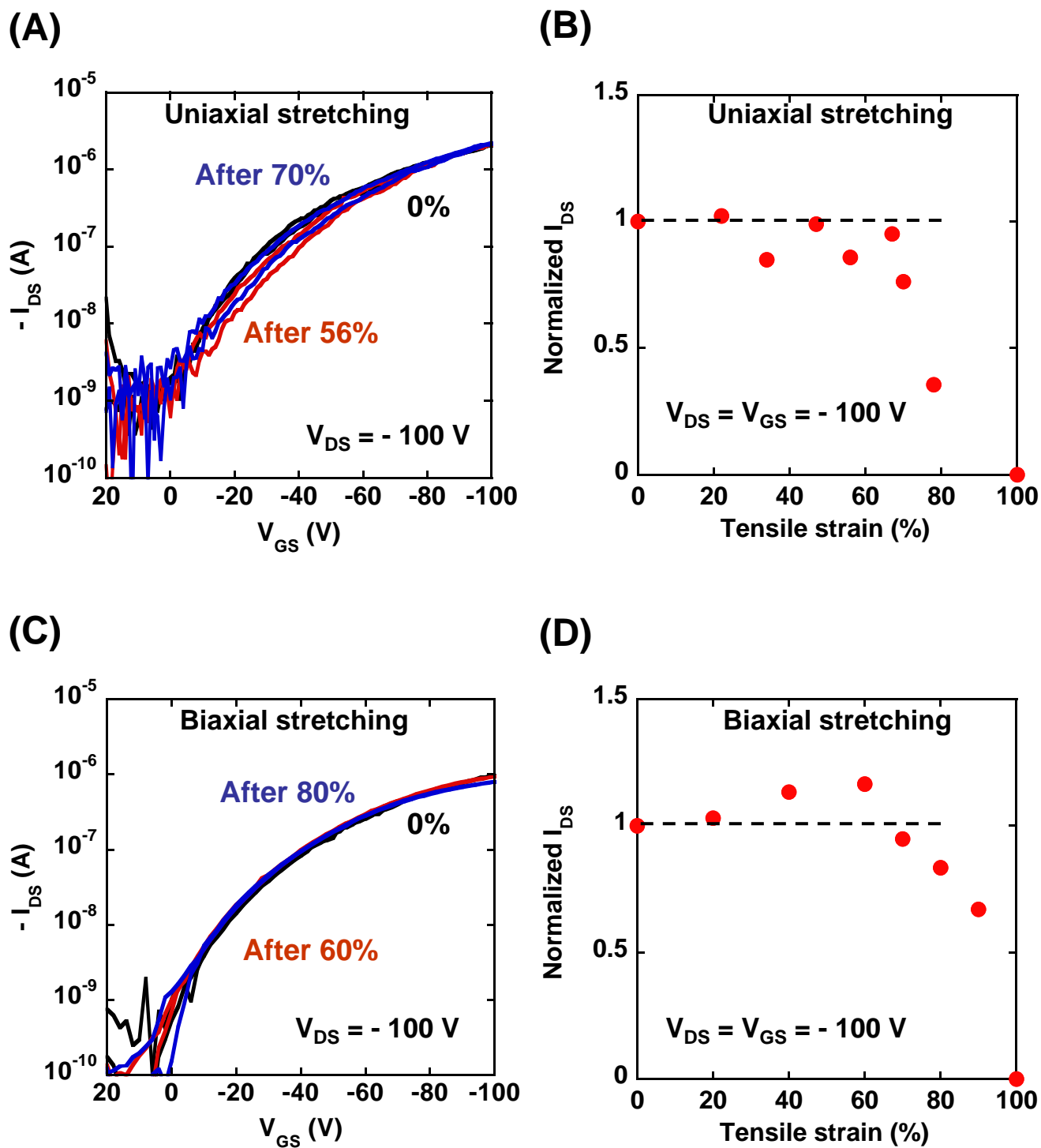
Fig. S13. Recovery performance after stretching.

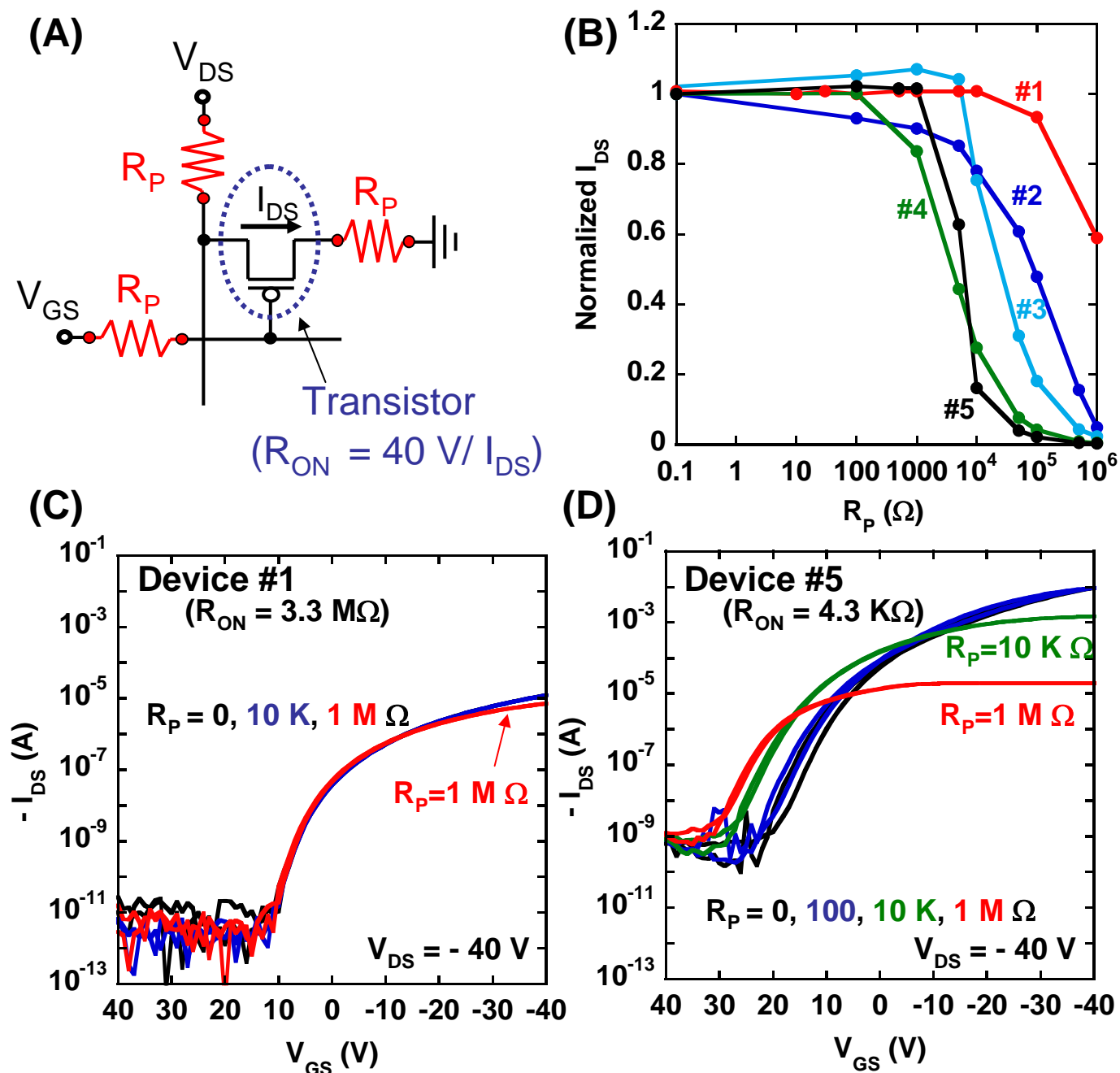| Device No.	I_{DS} (μA) ($V_{DS}=V_{GS}=-40$ V)	On-resistance of transistor (Ω)	W (μm)	L (μm)
#1	12.3	3.3 M	500	50
#2	200	200 K	2500	30
#3	850	48 K	10000	30
#4	4400	9.2 K	40000	30
#5	9300	4.3 K	90000	30

Fig. S14. Resistances of organic transistors and word and bit lines.